JOURNAL OF SOLID STATE CHEMISTRY 38, 199–210 (1981)

Neutron Powder Diffraction on $RbCrI_3$ and Magnetic Measurements on $RbCrI_3$ and $CsCrI_3$

H. W. ZANDBERGEN AND D. J. W. IJDO

Gorlaeus Laboratories, University of Leiden, P.O. Box 9502, 2300 RA Leiden, The Netherlands

Received August 20, 1980; in final form November 29, 1980

β-$RbCrI_3$ (a = 13.772(3), b = 8.000(2), c = 7.069(2) Å β = 95.85(1)°, Z = 4, $C2/m$ at 293 K) and γ-$RbCrI_3$ (a = 13.586(2), b = 7.923(2), c = 14.094(3) Å, β = 96.88(1)°, Z = 8, $C2$ at 1.2 K) are isostructural to β-$RbCrCl_3$ and γ-$RbCrCl_3$ and are both Jahn–Teller distorted $BaNiO_3$ structures. In both compounds elongated octahedra occur. γ-$RbCrI_3$ most probably has a magnetic spiral structure at 4.2 and 1.2 K. Theoretically, a spiral propagating along the b axis is expected. A model with $\mathbf{k}$ = 9/19$\mathbf{b}^*$ yielded the best result. However, no good fit was obtained possibly because of a misfit in $\mathbf{k}$ and canting of the magnetic moments due to anisotropy. χ vs T single-crystal measurements on β-$CsCrI_3$ are in accordance with its magnetic structure. The three-dimensional magnetic ordering temperature T_c is estimated as 27(1) K. From the χ vs T curves of γ-$RbCrI_3$, T_c could not be determined. From fits to χ vs T powder data J/k of $CsCrI_3$ and $RbCrI_3$ are estimated to be −14(2) and −11(1) K, respectively.

Introduction

Most $ACrX_3$ and $ACuX_3$ compounds (X = Cl, Br, or I; A = Rb or Cs) have $BaNiO_3$-type structures. In this type of structure the BX_6 octahedra share faces forming infinite chains along the c axis. A deformation with respect to the $BaNiO_3$ structure due to the cooperative Jahn–Teller effect has been reported for several compounds. $CsCuCl_3$ has a phase transition at 420 K (α-$CsCuCl_3$ ($P6_3/mmc$) (*1*) → β-$CsCuCl_3$ ($P6_122$) (*1*, *2*)). $RbCrCl_3$ has two phase transitions, a second-order one in the temperature range 300–400 K (*3*) and a first-order one at 195 K (α-$RbCrCl_3$ (probably $P6_3/mmc$) → β-$RbCrCl_3$ ($C2/m$) (*4*) → γ-$RbCrCl_3$ ($C2$) (*5*)). The structure of β-$RbCrCl_3$ can be regarded (*3*) as a random structure of γ-$RbCrCl_3$. The phase transition (α-$CsCrCl_3$ ($P6_3/mmc$) (*6*) → β-$CsCrCl_3$ ($C2$) (*3*)) takes place at 170 K. Crama (*3*) reported β-$CsCrCl_3$ to be isomorphous to γ-$RbCrCl_3$. However, the monoclinic angle is 88.63(3)° (at 60 K) compared to 93.94(4)° (at 100 K) for γ-$RbCrCl_3$. No phase isomorphous to β-$RbCrCl_3$ occurs (*3*). Day *et al.* (*7*) claimed β-$CsCrCl_3$ to be triclinic; however, no doubling of the c axis is reported. $CsCrI_3$ has a phase transition at 150 K (α-$CsCrI_3$ ($P6_3/mmc$) (*6*, *8*) → β-$CsCrI_3$ ($Pbcn$) (*8*)). X-Ray single-crystal diffraction on α-$CsCuCl_3$, α-$CsCrCl_3$ and α-$CsCrI_3$ (*1*, *6*) show these phases to have Jahn–Teller deformed octahedra.

In all these Jahn–Teller deformed structure types elongated octahedra occur. Except for β-$CsCuCl_3$ (shifts perpendicular to the c axis), in all structure types the elongation is obtained mainly by shifts along the c axis. Denoting the axes of an octahedron by x, y, and z, an elongation along one of these

0022-4596/81/080199-12$02.00/0

axes can be represented by x, y, or z. Using for the other octahedra the same notation (see Fig. 1), the cooperative Jahn–Teller deformation can be represented by the axes of elongation: β-$CsCuCl_3$, $xyzxyz$; γ-$RbCrCl_3$, $xyxz$; β-$RbCrCl_3$, $x(y$ or $z)$; β-$CsCrI_3$, xy; α-$CsCuCl_3$, α-$CsCrCl_3$, and α-$CsCrI_3$, $(x,y$ or $z)$, where $x,(y$ or $z)$ represents a chain of octahedra with the nth octahedron elongated along the x axis, the $(n + 1)$th along y or z, the $(n + 2)$th along x, etc.

The magnetic properties of ABX_3 compounds with the $BaNiO_3$ structure have been studied extensively because of their quasi-one-dimensional behavior. For β-$RbCrI_3$ at 293 K the distance between nearest neighbor Cr^{2+} ions is 3.53 Å in the chain and 8.00 Å between two chains. Most compounds with this structure have a strong antiferromagnetic intrachain exchange interaction. With ferromagnetic interchain exchange, a spin structure with ferromagnetic planes coupled antiferromagnetically will be obtained, viz, $CsCrI_3$ (*8*). When the interchain exchange is antiferromagnetic and equal between all neighboring chains a 120° structure occurs when magnetic anisotropy is small ($CsMnI_3$: magnetic moments in a plane perpendicular to the basal plane (*9*) $CsVI_3$: magnetic moments in the basal plane (*10*)), and a collinear magnetic structure when the anisotropy is large ($CsCoCl_3$: magnetic moments along the c axis (*11*)).

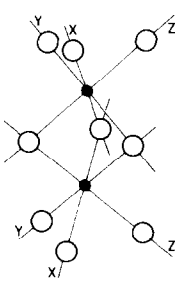

FIG. 1. The definition of the axes of two neighbor CrI_6 octahedra.

In an earlier paper (*8*) the determination of the crystal structures of α-$CsCrI_3$ and β-$CsCrI_3$, and the magnetic structure of β-$CsCrI_3$ at 1.2 K were reported. In this paper the structure determinations of β-$RbCrI_3$ and γ-$RbCrI_3$ and magnetic measurements on tripletted crystals of γ-$RbCrI_3$ and β-$CsCrI_3$ are reported.

Experimental

The sample of $RbCrI_3$ used for neutron diffraction was prepared by first melting a stoichiometric mixture of the binary compounds. The mixture was then powdered and annealed for a week at 350°C in an evacuated glass tube several times. CrI_2 was prepared from the elements and was purified by sublimation. RbI (p.a.) and CsI (p.a.) purchased from Merck were used.

Neutron powder diffraction diagrams of $RbCrI_3$ were recorded at 293, 4.2, and 1.2 K at the HFR reactor at Petten (the Netherlands) using $\lambda = 2.5754(3)$ Å with 30° collimation in the angular range $4° < 2\Theta < 140°$. For the refinements the profile program of Rietveld (*12*) was used. No absorption correction was applied. The coherent scattering lengths used are (*13*) $b(Rb) = 0.71$, $b(Cr) = 0.352$, and $b(I) = 0.53$ all in units of 10^{-12} cm. The magnetic form factors were taken from Watson and Freeman (*14*).

Single crystals of $CsCrI_3$ and $RbCrI_3$ were grown using the Bridgman method. Single crystals of both compounds are easily cleaved along the (1 1 0) plane. Because of the phase transitions no single crystals of β-$CsCrI_3$ and β-$RbCrI_3$ could be obtained. X-Ray Weissenberg photographs taken at 293 K (β-$RbCrI_3$) and 100 K (γ-$RbCrI_3$ and β-$CsCrI_3$) of small crystals show the crystals to be "tripletted," with an equal occurrence for the three domains. This complicates the interpretation of the magnetic measurements. For instance, when for β-$CsCrI_3$, a magnetic field **H** is applied perpendicular to (1 1 0) of the high-temperature

phase, this implies that about $\frac{1}{3}$ of the domains are oriented with their a axis along **H** and that $\frac{2}{3}$ of the domains will have their a axis making an angle of 60° with **H**. In the following, the expression "tripletted crystal" will be used for such a collection of domains.

DTA measurements show $RbCrI_3$ to have a phase transition at 223 K. No phase transition above 293 K could be detected.

Susceptibility vs temperature measurements in the region 2–100 K and magnetization vs magnetic field measurements were carried out on tripletted crystals of $RbCrI_3$ (100 mg) and $CsCrI_3$ (205 mg) by means of a Vibrating Sample Magnetometer (*15*), equipped with a superconducting magnet supplying fields up to 56 kOe. χ vs T measurements in the region 80–300 K were performed on powders using the Faraday method.

Results of Neutron Diffraction on $RbCrI_3$

X-Ray rotation and Weissenberg photographs of $RbCrI_3$ at 293 and 100 K suggest the compound to be monoclinic at both temperatures and to have a doubled c axis at 100 K. Guen *et al.* (16) report a triclinic unit cell for $RbCrI_3$ at room temperature (a = 8.047(8), b = 8.057(8), c = 7.261(13) Å α = 90.38(14), β = 95.69(16), γ = 120.70(7)°). However, the Weissenberg photographs, taken by us, are not in accordance with this unit cell. They show an angle of about 96° to exist between [0 0 1] and [1 0 0] of the quasi-hexagonal unit cell. Because $RbCrCl_3$ shows a similar behavior the refinement on the neutron diffraction data recorded at 293 K were started with the positions of β-$RbCrCl_3$. Full-matrix refinement led to convergence at

$$R(\text{total}) = \sum_i |I_i(\text{obs}) - (1/c)I_i(\text{calc})| / \sum_i I_i(\text{obs}) = 0.062$$

and

$$R(\text{profile}) = \left[\sum_j w_j\{y_j(\text{obs}) - (1/c)y_j(\text{calc})\}^2 / \sum_j w_j y_j(\text{obs})^2\right]^{1/2} = 0.129,$$

where I_i is the intensity of the ith reflection, y_j the intensity of the jth measuring point, c a scaling factor, and w_j a statistical weight factor. In this model elongated and shortened octahedra occur. Because only elongated octahedra are expected the I(2) ions were distributed over two equally occupied positions: I(2a) and I(2b). Refinement with this model led to lower R values (R(total) = 0.057 and R(profile) = 0.127) and significant shifts of I(2a) and I(2b). The shifts of the two parts were negatively coupled in this refinement. The largest shift is found along the c axis, in accordance with the anisotropic thermal parameters of β-$RbCrCl_3$ (*4*). The observed and calculated profiles are shown in Fig. 2 and the final parameters are given in Table I.

The neutron powder diffraction diagrams recorded at 4.2 and 1.2 K contain a number of magnetic reflections. The positions of these reflections are the same for both temperatures, whereas the intensities have an equal magnitude. These reflections can not be indexed by means of simple multiples of the axes of the nuclear unit cell. Because of competing exchange interactions a spiral structure can be expected for γ-$RbCrI_3$. Such a structure can be described by a vector **k** in the reciprocal space.

Because the exact position of only a few magnetic reflections is known, the direction and the length of **k** are very difficult to establish. This is further complicated by the fact that the unit cell is monoclinic. Neutron diffraction was done on a tripletted crystal in order to establish **k**. However, no significant reflections were observed, prob-

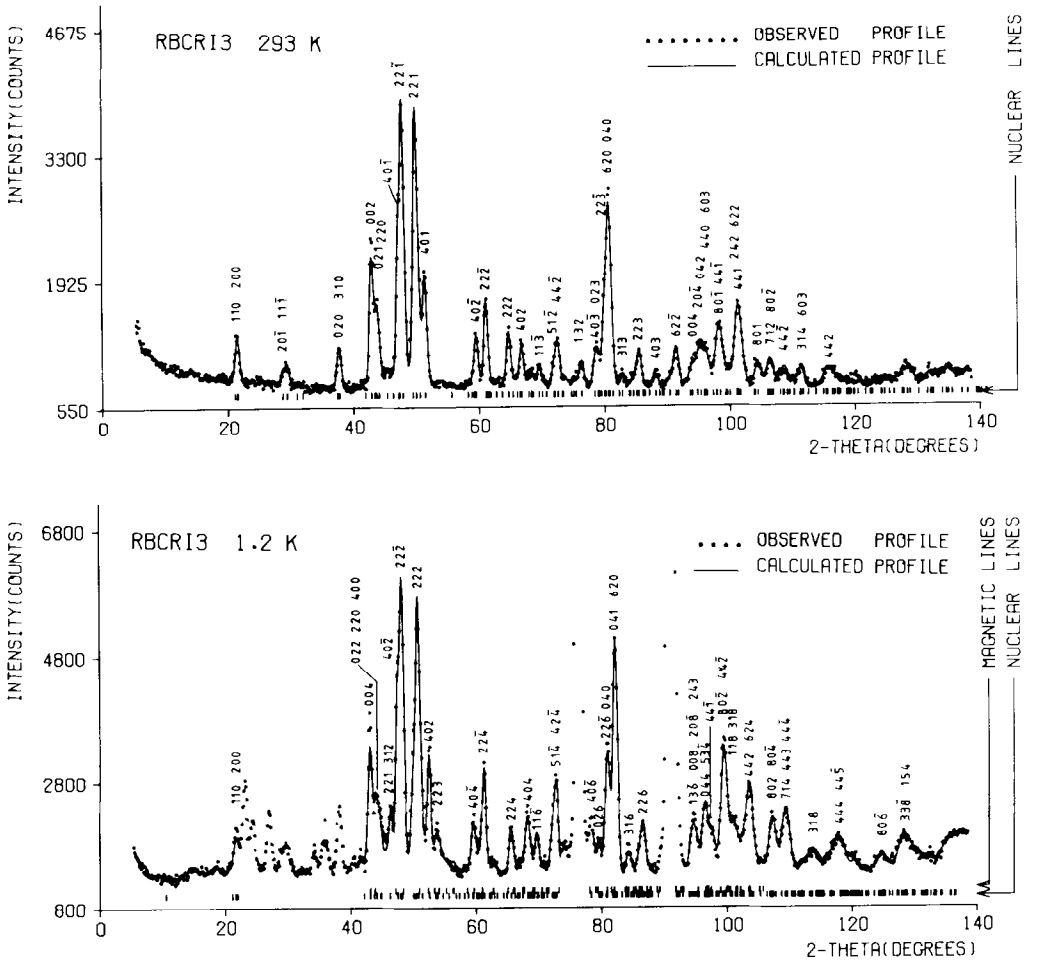

FIG. 2. The observed and calculated profiles of β-$RbCrI_3$ at 293 K (top) and γ-$RbCrI_3$ at 1.2 K (bottom). The 2Θ region 22–44° of the recording at 1.2 K is excluded.

ably because the occurrence of domains leads to very broad peaks. Therefore, since a spiral structure has to originate in competing exchange interactions, we have tried to determine the nature of the exchange interactions occuring in this compound.

Susceptibility measurements show the compound to be a quasi-one-dimensional antiferromagnet. The most important exchange interaction will be cation–cation exchange via the t_{2g} orbitals of nearest neighbor Cr^{2+} ions in the chain. This exchange interaction causes the one-dimensional character of $RbCrI_3$. Since this exchange interaction is very strong no component of **k** is expected in the c* direction.[1] Moreover, no spiral structures with a component of **k** along c* has been observed for ABI_3 compounds with the $BaNiO_3$ structure. Because of this, the spiral structure must be caused by competing interchain exchange interactions. For compounds with the undistorted $BaNiO_3$ structure two types of interchain exchange interactions

[1] Smart (*17*) showed that a spiral along a chain is to be expected if $|J_N| < 4|J_{NN}|$ and J_{NN} is antiferromagnetic, where J_N and J_{NN} are the nearest and next nearest neighbor exchange interaction in the chain, respectively.

TABLE I

POSITIONAL AND ISOTROPIC THERMAL PARAMETERS ($b = 8(\pi \bar{U})^2$ Å^2 (20)) AND THE UNIT CELL DIMENSIONS OF $RbCrI_3$ AT 293 AND 1.2 K

	x	y	z	b
	β-$RbCrI_3$[a](293 K) $a = 13.772(3)$, $b = 8.000(2)$, $c = 7.069(2)$ Å, $\beta = 95.85(1)°$			
Rb	−0.3384(7)	0	0.7430(11)	5.7(3)
Cr(1)	0	0	0	3.7(3)
Cr(2)	0	0	0.5	
I(1)	0.1686(6)	0	0.1820(13)	3.0(3)
I(2)	0.0839(5)	0.2446(12)	0.7120(8)	4.6(2)
I(2a)	0.0857(13)	0.2576(26)	0.6856(30)	3.2(3)
I(2b)	0.0827(13)	0.2331(26)	0.7384(30)	
	γ-$RbCrI_3$ (1.2 K) b(overall) = 0.1(1) Å^2, $a = 13.586(2)$, $b = 7.923(2)$, $c = 14.094(3)$ Å, $\beta = 96.88(1)°$			
Rb(a)	0.350(2)	0.036(4)	0.391(2)	
Rb(b)	0.326(2)	0.015(4)	0.876(2)	
Cr(1a)	0	0	0	
Cr(1b)	0	0.063(6)	0.5	
Cr(2)	−0.002(3)	0.035(6)	0.249(4)	
I(1a)	0.166(3)	0.023(6)	0.164(4)	
I(1b)	0.176(3)	0.061(5)	0.667(4)	
I(2a)	0.085(3)	0.310(7)	0.401(4)	
I(2b)	0.089(4)	0.252(7)	0.909(4)	
I(3a)	0.085(4)	−0.185(6)	0.391(3)	
I(3b)	0.082(4)	−0.254(9)	0.881(3)	

[a] For β-$RbCrI_3$, the positions of I(2) and the divided I(2); I(2a) and I(2b), are given.

via two anions occur viz J_a and $J_{a'}$ (see Fig. 3). The same exchange interactions in equal occurrence exist between the three chains I, II and III (Fig. 4) resulting in a 120° structure when the effective exchange interaction is antiferromagnetic and the anisotropy is small. The γ-$RbCrI_3$ the effec-

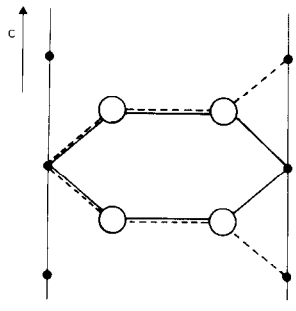

FIG. 3. The interchain exchange paths of J_a (full drawn) and $J_{a'}$ (dashed). The small black circles represent the Cr^{2+} ions and large circles the I^- ions.

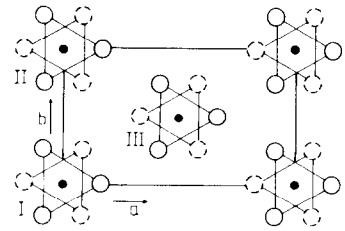

FIG. 4. The definition of the chains I, II, III. The small black circles represent Cr^{2+} ions at $z \approx 0$ and 0.5. The full-drawn and dashed large circles represent I^- ions on $z \approx 0.25$ and 0.75, respectively.

tive exchange interactions between the chains will be different since the exchange paths vary due to the Jahn–Teller distortion. With a fully antiparallel orientation in the chain, the effective exchange interaction between the chains I and III, J(I,III), is equal to J(II,III) and differs from J(I,II). A component of **k** in the **a*** direction can occur only if the exchange interactions J(I,III) and J(II,III) are different. Therefore **k** is expected to be parallel to **b***. The sign of J(I,II) and J(I,III) will determine which of the four magnetic structures shown in Fig. 5 will occur. The two collinear structures are not in accordance with the neutron diffraction diagrams, leaving the two spiral structures to be investigated.

Two magnetic models based on the assumptions above were refined, viz, Model A (first magnetic reflection: $\{0\ 0\ l^{\pm}\}$) with J(I,II) antiferromagnetic and J(I,III) ferromagnetic with **k** = 9/19 **b*** and Model B (first magnetic reflection $\{0\ 1\ l^{-}\}$) with J(I,II) and J(I,III) both antiferromagnetic and **k** = 9/19 **b***. Because no incommensurable vector **k** can be introduced in the profile refinement program used, **k** is taken as a fraction. In the models the magnetic moments are oriented in such a way that along the y direction the magnetic moment of each next Cr^{2+} ion is rotated by (9/19) × 360°.

Refinements were done on both models with the magnetic moments in the planes (1 0 0), (0 1 0), and (0 0 1) and three planes making an angle of 45° around the a and the

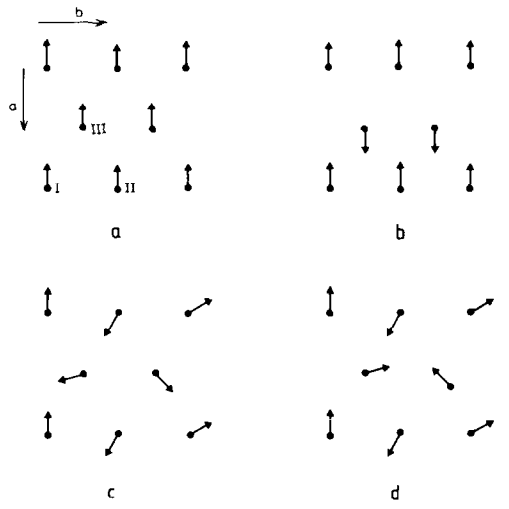

FIG. 5. The four magnetic structures expected for γ-$RbCrI_3$: (a) J(I,II) and J(I,III) ferromagnetic; (b) J(I,II) ferromagnetic and J(I,III) antiferromagnetic; (c) J(I,II) antiferromagnetic and J(I,III) ferromagnetic; (d) J(I,II) and J(I,III) antiferromagnetic.

b (+45° and −45°) axis with the (0 0 1) plane. The best fit was obtained for Model A with the magnetic moments in the (0 0 1) plane. However, the fit is still very poor. Positional misfits can be caused partly by the refinement program used, which does not allow the refinement of **k**. These misfits might also be caused by **k**, deviating from the **b*** direction. As discussed above this is not to be expected. Also, no satisfactory results were obtained when we tried to index the observed magnetic reflections by means of a vector **k**, being not parallel to **b***. Furthermore, a deviation of **k** from the **b*** direction would give rise to a broadening of the magnetic reflections if the deviation is small or to extra reflections when the deviation is large. Only a small number of unbroadened magnetic reflections occur in the diffraction diagram. The misfit in the ratio of the intensities of the magnetic reflections can be caused by a canting of the magnetic moments towards an easy axis due to anisotropy.

Further, a Model C was refined having a doubled b-axis and an antiparallel sequence of the magnetic moments along the b and the c axis. The directions of the magnetic moments of the Cr^{2+} ions on the positions 0,0,0 and 0.5,0.5,0 were refined independently. This model does not have a spiral structure. The magnetic moments were refined to be in the (0 0 1) plane (within the standard deviation), with one being almost parallel to the a axis and the other making an angle of 30° with the a axis. This result suggests the a axis to be the easy direction and is an indication that the magnetic moments in models A and B should be canted towards the a axis. The magnetic moments were refined to 2.4(1), 2.3(1), and 1.8(1) μ_B for the Models A, B, and C, respectively.

No further efforts were made to determine the magnetic structure of γ-$RbCrI_3$ because of the complexity of the problem and the low number of significant magnetic reflections. Because of the poor fit, another refinement was done excluding the region with the strong magnetic reflections (22–44°). For Model A, with the magnetic moments fixed to 2.4 μ_B in (0 0 1), the positional parameters were refined. The results of the refinement on the recording at 1.2 K are listed in Table I. The observed and calculated profiles of the recording at 1.2 K are depicted in Fig. 2.

Magnetic Measurements

$CsCrI_3$

Magnetization vs magnetic field measurements were carried out on a tripletted crystal of $CsCrI_3$ at 4.2 K in three orthogonal directions with **H** parallel to [0 0 1], [1 0 0], and [1 1 0] of the hexagonal unit cell of α-$CsCrI_3$. No difference was found between the measurements with **H** parallel to [1 0 0] and [1 1 0]. Along all three directions dM/dH showed no field dependence up to H = 56 kOe.

χ vs T measurements were performed in

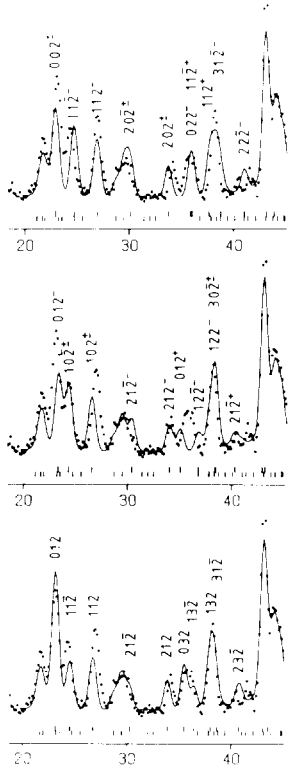

FIG. 6. The fits in the 2Θ region 20–44° of the Models A, B, and C. The experimental data are indicated by points and the calculated profile by a full-drawn curve. Below the figures the positions of the nuclear and magnetic reflections are given similar to Fig. 2.

the same three directions. No difference was measured between $\chi(\|[100])$ and $\chi(\|[110])$. The curves of $\chi(\|[001])$ and $\chi(\|[100])$ are shown in Fig. 7. The curve of $\chi(\|[100])$ shows a sharp change in slope at 27(1) K, which temperature is taken to be the three-dimensional transition temperature T_c. A large difference is found between the susceptibilities parallel and perpendicular to the c axis. The increase of χ below 6 K is ascribed to paramagnetic impurities. Above 40 K, an isotropic susceptibility is observed.

Additional χ vs T measurements in the temperature region 80–300 K are performed on a powder of $CsCrI_3$. The χ vs T and $1/\chi$

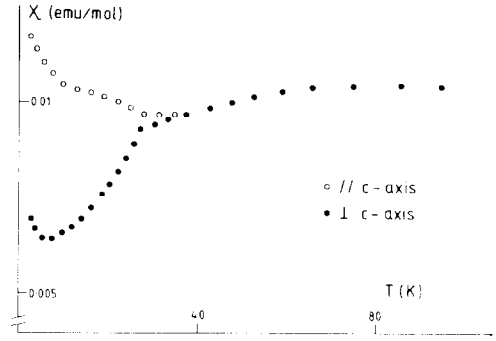

FIG. 7. χ vs T curves of $CsCrI_3$ measured in a magnetic field of 5 kOe.

vs T curves are depicted in Fig. 8. The χ vs T curve was fitted using $g = 1.97$ and $S = 2$ with series expansion according to Wood and Dalton (*18*). No good fit was obtained as can be seen from Fig. 7, possibly because of the phase transition. Near the phase transition temperature (150 K) a change in the slope of $1/\chi$ is observed, suggesting differences in the interactions above and below the phase transition. From the slope of $1/\chi$ vs T at high temperature Θ and μ(eff) were determined to be $-160(10)$ K and 4.92(5) μ_B. The spin-only value is 4.90 μ_B.

$RbCrI_3$

M vs **H** measurements were carried out

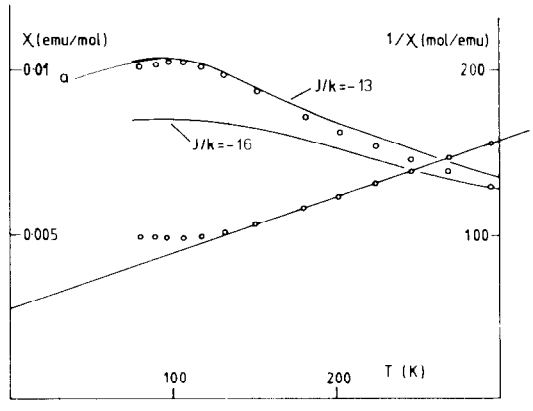

FIG. 8. χ vs T and $1/\chi$ vs T curves measured by means of the Faraday method. Curve a represents the single-crystal measurements.

on a tripletted crystal of $RbCrI_3$ at 4.2 K with **H** parallel to [0 0 1], [1 0 0] and [1 1 0] of the hexagonal unit cell. No difference was found between the measurements with **H** parallel to [1 0 0] and [1 1 0]. dM/dH was found to be independent on H up to 56 kOe.

χ vs T measurements were done in the same directions. $\chi(\|[100])$ and $\chi(\|[110])$ are equal within experimental accuracy. The curves of $\chi(\|[001])$ and $\chi(\|[100])$ are shown in Fig. 9. From the neutron diffraction experiments it is found that T_c must be considerably higher than 4.2 K. T_c could not be determined from the χ vs T curves. Above 45 K an isotropic behavior is observed.

χ vs T measurements between 80 and 300 K are shown in Fig. 9. These data could be fitted best with $J/k = -11$ K using $g = 1.97$ and $S = 2$ in series expansion according to Wood and Dalton. The fit is shown in Fig. 10. Similar to $CsCrI_3$ a phase transition occurs ($T = 223$ K) in the temperature region of the fit. From the slope of $1/\chi$ vs T at high temperature Θ and μ(eff) are determined as -95 K and 4.85 μ_B, respectively.

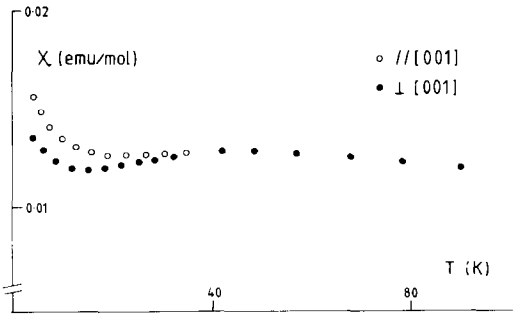

FIG. 9. χ vs T curves of $RbCrI_3$ measured in a magnetic field of 5 kOe.

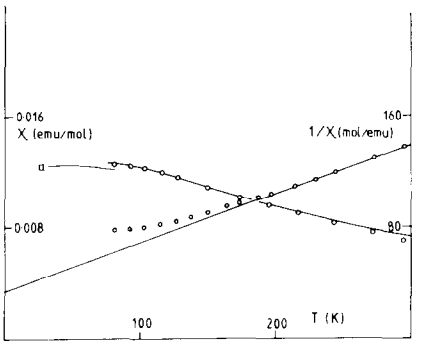

FIG. 10. χ vs T and $1/\chi$ vs T curves of $RbCrI_3$ (Faraday method). The full-drawn curve through the χ vs T points represents the fit with $J/k = -11$ K. Curve a represents the single-crystal measurements.

Discussion

β-$RbCrI_3$ and γ-$RbCrI_3$ have Jahn–Teller distorted $BaNiO_3$ structures. Compared to the transition temperature of α-$CsCrI_3 \rightarrow \beta$-$CsCrI_3$ (150 K) the phase transition α-$RbCrI_3 \rightarrow \beta$-$RbCrI_3$ (above 293 K) takes place at a much higher temperature, which is caused by the smaller radius of the Rb^+ ion. Since Rb^+ is too small for a 12 coordination of I^- ions, the transition to the low-temperature phases, with Rb in a 9 coordination (see Tables II and III) will take place at a higher temperature. Another distorted $BaNiO_3$ structure is found for $RbVI_3$, the distortion of which is also due to the smaller radius of Rb^+ (*10*).

Whereas in γ-$RbCrI_3$ only elongated octahedra occur, the results of the refinement of β-$RbCrI_3$ with a nondistributed I(2) suggest the existence of elongated and shortened octahedra (see Table III). However,

TABLE II

SOME DISTANCES (Å) IN β-$RbCrI_3$ AT 293 K

Rb–I(1)	3.69(1)	Rb–I(2a)	4.10(2)
Rb–I(1)	4.03(1) 2×	Rb–I(2a)	3.90(2)
Rb–I(2)	4.04(1) 2×	Rb–I(2a)	3.67(2)
Rb–I(2)	3.93(1) 2×	Rb–I(2b)	3.99(2)
Rb–I(2)	3.86(1) 2×	Rb–I(2b)	3.98(2)
		Rb–I(2b)	4.07(2)
Cr(1)–I(1)	2.77(1) 2×	Cr(2)–I(1)	3.06(1) 2×
Cr(1)–I(2)	2.97(1) 4×	Cr(2)–I(2)	2.79(1) 4×
Cr(1)–I(2a)	3.17(2)	Cr(2)–I(2a)	2.77(2)
Cr(1)–I(2b)	2.79(2)	Cr(2)–I(2b)	2.83(2)

Note. I(2a) and I(2b) are parts of the divided I(2) ion.

TABLE III

SOME DISTANCES (Å) IN γ-$RbCrI_3$ AT 1.2 K

Rb(a)–I(1a)	3.82(5)	Rb(b)–I(1a)	4.07(6)
Rb(a)–I(1b)	4.25(5)	Rb(b)–I(1b)	3.94(6)
Rb(a)–I(1b)	3.85(5)	Rb(b)–I(1b)	3.40(5)
Rb(a)–I(2a)	4.23(6)	Rb(b)–I(2b)	3.80(6)
Rb(a)–I(2a)	3.64(6)	Rb(b)–I(2b)	4.12(6)
Rb(a)–I(2a)	3.45(6)	Rb(b)–I(2b)	3.74(6)
Rb(a)–I(3a)	3.96(6)	Rb(b)–I(3b)	3.90(6)
Rb(a)–I(3a)	3.94(6)	Rb(b)–I(3b)	5.97(6)
Rb(a)–I(3a)	3.85(5)	Rb(b)–I(3b)	3.99(6)
Cr(1a)–I(1a)	3.03(4) 2×	Cr(2)–I(1a)	2.70(7)
Cr(1a)–I(2b)	2.73(6) 2×	Cr(2)–I(1b)	2.78(7)
Cr(1a)–I(3b)	2.86(6) 2×	Cr(2)–I(2a)	3.18(7)
		Cr(2)–I(2b)	2.93(7)
Cr(1b)–I(1b)	3.14(5) 2×	Cr(2)–I(3a)	2.76(7)
Cr(1b)–I(2a)	2.74(7) 2×	Cr(2)–I(3b)	3.00(8)
Cr(1b)–I(3a)	2.76(6) 2×		

the refinement of β-$RbCrI_3$ with a divided I(2) results in lower R values and Cr–I distances, which strongly suggest the existence of elongated octahedra only. Contrary to γ-$RbCrI_3$, this elongation is obtained mainly by shifts of I(2) along the c axis. Because of this difference, it must be noted that the structure of β-$RbCrI_3$ cannot be regarded as a random γ-$RbCrI_3$ structure. It is concluded that the deformation with respect to the $BaNiO_3$ structure can be represented by x(y or z) and $xyxz$ for β-$RbCrI_3$ and γ-$RbCrI_3$, respectively.

The χ vs T curves of β-$CsCrI_3$ are in good agreement with the magnetic structure (*8*) (see Fig. 11). Taking into account the tripletting due to the phase transition the spin orientations as shown in Fig. 12 will occur in the tripletted crystal.

When the anisotropy is small a spin-flop transition for a part of the magnetic moments is expected when a magnetic field is applied along [1 1 0] of the hexagonal unit cell. Since no field dependence is found for dM/dH with **H** parallel to [1 0 0] or [1 1 0] in fields up to 56 kOe, no spin-flop transition is expected below 100 kOe and H_A/H_E is estimated to be larger than 0.005 (using $H_{SF} = (2H_AH_E - H_A^2)^{1/2}$), where H_A is the anisotropy field and H_E the exchange field.

Because of the strong intrachain exchange interaction the orientation of the magnetic moments in a low magnetic field will be almost equal to the one in zero field (see Fig. 12). Using the spin orientations in zero field and denoting the susceptibilities of a single crystal of β-$CsCrI_3$ along the three orthorhombic axes by $\chi(\|a)$, $\chi(\|b)$, and $\chi(\|c)$ the measured susceptibilities of the tripletted crystal will be

$$\chi(\|[001]) = \chi(\|c),$$

$$\chi(\|[100]) = \chi(\|[110]) = 0.5\chi(\|a) + 0.5\chi(\|b).$$

With $\chi(\|a)$ vanishing at $T = 0$, $\chi(\|[100])$ will be $0.5\chi(\|b)$. With $\chi(\|c) \approx \chi(\|b)$ the expected ratio of $\chi(\|[001])/\chi(\|[100])$ will be close to 0.5, which value is also found by extrapolation of the experimental data to $T = 0$.

The ratio $\chi(\|[001])/\chi(\|[100])$ is much larger for γ-$RbCrI_3$: 0.85. This behavior, which was found for other tripletted crystals of γ-$RbCrI_3$ as well, can be understood if one assumes that the magnetic moments

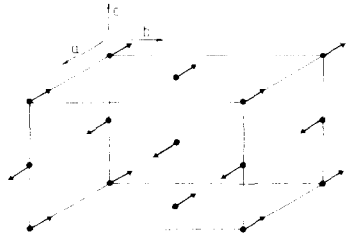

FIG. 11. The magnetic structure of β-$CsCrI_3$.

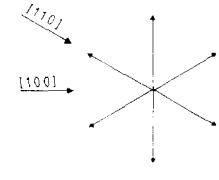

FIG. 12. The orientation of the magnetic moments in a tripletted crystal of β-$CsCrI_3$.

of a part of the Cr^{2+} ions have a component parallel to the c axis. In order to test this, three spin planes, making an angle of 45° with the c axis, were introduced in the neutron diffraction refinement; however, without satisfactory results. No better ratio of the magnetic reflections was obtained.

Whereas the compounds $RbVI_3$, $CsVI_3$, and $CsMnI_3$ have a 120° sturcture, β-$CsCrI_3$ has a collinear structure. Between the chains two types of exchange interactions occur: J_a and $J_{a'}$ (see Fig. 4). The exchange paths of J_a and $J_{a'}$ can be characterized as a 180°–180° and a 180°–90° exchange path (see Fig. 13), respectively. J_a and $J_{a'}$ exist between the chains in equal occurrence. Because of the antiparallel sequence of magnetic moments within the chain, J_a and $J_{a'}$ must be unequal to obtain an effective exchange interaction between the chains. Since more orbitals are involved in the exchange mechanism of $J_{a'}$, $J_{a'}$ is expected to be smaller than J_a.

Goodenough (*19*) shows that the exchange interaction between two magnetic ions depends on the occupation of the d orbitals of the magnetic ions participating in the exchange mechanism. For a 180° super exchange Goodenough predicts: exchange interaction via two empty orbital (EE): moderately antiferromagnetic; via an empty and a half-filled orbital (EH); moderately ferromagnetic; via two half-filled orbitals (HH): strongly antiferromagnetic.

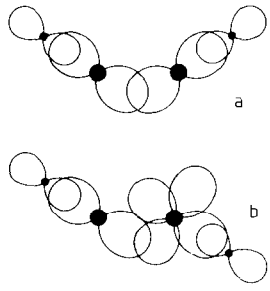

FIG. 13. The exchange paths of J_a (a) and $J_{a'}$ (b).

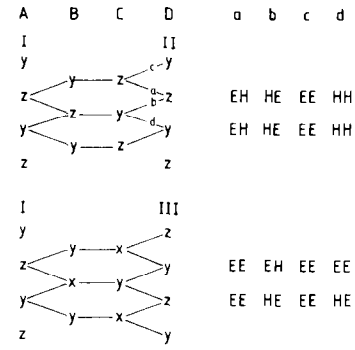

FIG. 14. The orbital occupation of the Cr^{2+} ions in β-$CsCrI_3$, which are participating in the exchange mechanism. A and D represent the elongation directions of the CrI_6 octahedra along the chains. B and C represent the positions of the intermediate I^- ions with respect to the axes of the CrI_6 octahedra in the chains I and II (or III), respectively. For instance EH implies an exchange path via an empty and a half-filled orbital.

180°–180° exchange interactions are predicted to be much smaller but of equal sign.

Assuming that J_a is dominating in the effective interchain exchange interaction the magnetic structures of $RbVI_3$ and $CsVI_3$ (EE interactions) and $CsMnI_3$ and $CsFeI_3$ (HH interactions) are in accordance with the predictions of Goodenough. In β-$CsCrI_3$ three types of exchange interactions occur, EE, EH, and HH, as is shown in Fig. 14. The effective interchain exchange between the chains I and II, J(I,II) is expected to be ferromagnetic, whereas J(I,III) is expected to be either weakly ferromagnetic or weakly antiferromagnetic. Neutron diffraction experiments show both J(I,II) and J(I,III) to be ferromagnetic.

Using these results it is interesting to consider the exchange paths in γ-$RbCrI_3$ in order to obtain a prediction for the magnetic structure. The exchange paths are depicted in Fig. 15. The paths between II and III are similar to those between I and III except for a contrary sequence. (The twofold axis generates I–III into II–III, yielding J_1, J_2, J_3, J_4, J_1, J_2, etc. for I–III and J_1, J_4, J_3, J_2, J_1, J_4, etc. for II–III.) For

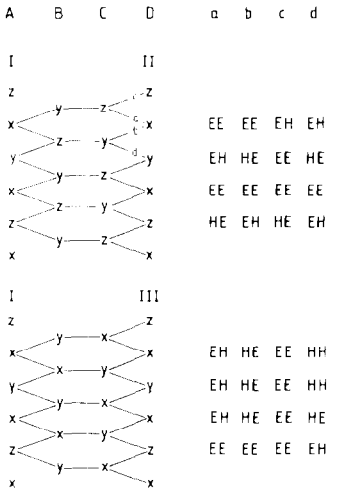

FIG. 15. The orbital occupation of the Cr^{2+} ions in γ-$RbCrI_3$, which are participating in the interchain exchange mechanism. The representation is given in Fig. 14.

I–II the sum of the exchange interactions of the J_a type contains EE and EH exchange paths in equal amounts, while the EH exchange paths are dominating for I–III. Using the results obtained for β-$CsCrI_3$ it is to be expected that J(I,III) is ferromagnetic and J(I,II) weakly ferromagnetic, yielding a collinear structure. Since the exchange paths are different in both compounds J(I,II) can also be weakly antiferromagnetic yielding a spiral structure, with a spiral propagating along the b axis. The observed magnetic reflections could not be indexed satisfactorily when it was assumed that J(I,III) is moderately ferromagnetic and J(I,II) is weakly antiferromagnetic. Model A which was refined implicates that J(I,II) is antiferromagnetic and J(I,III) ferromagnetic and that $|J(\text{I,II})| > |J(\text{I,III})|$.

Day *et al.* (*7*) reported the magnetic structure of β-$CsCrCl_3$ to consist of an antiferromagnetic spin alignment in the pseudohexagonal y and z directions and a ferromagnetic alignment along the a axis, with the spins in the basal plane. Unfortunately they do not report the direction of the ferromagnetic alignment in the basal plane with respect to the claimed triclinic unit cell of β-$CsCrCl_3$, the positional parameters and the R values. Furthermore, no doubling of the c axis is reported. This makes comparison with our results difficult. It is our guess that β-$CsCrCl_3$ is monoclinic, as found by Crama (*3*), and that the magnetic structure is such that a ferromagnetic alignment occurs along the y direction of the monoclinic unit cell. This magnetic structure occurs when J(I,II) is ferromagnetic and J(I,III) antiferromagnetic (b in Fig. 5).

Acknowledgments

The authors wish to thank Dr. L. J. de Jongh and Dr. D. W. Engelfriet for helpful discussions and a critical reading of the manuscript, and Mr. J. Strang of the Energienderzoek Centrum Nederland for performing the neutron diffraction experiments.

References

1. W. J. CRAMA, *Acta Crystallogr.*, in press.
2. A. W. SCHLUETER, R. A. JACOBSON, AND E. E. RUNDLE, *Inorg. Chem.* **5**, 277 (1966).
3. W. J. CRAMA, Thesis, Leiden (1980).
4. W. J. CRAMA, W. J. A. MAASKANT, AND G. C. VERSCHOOR, *Acta Crystallogr. Sect. B* **34**, 1973 (1978).
5. W. J. CRAMA, M. BAKKER, G. C. VERSCHOOR, AND W. J. A. MAASKANT, *Acta Crystallogr. Sect. B* **35**, 1875 (1979).
6. W. J. CRAMA AND H. W. ZANDBERGEN, *Acta Crystallogr.* in press.
7. P. DAY, A. K. GREGSON, D. H. LEECH, M. T. HUTCHINGS, AND B. D. RAINFORD, *J. Magnet. Magnet. Mater.* **14**, 166 (1979).
8. H. W. ZANDBERGEN AND D. J. W. IJDO, *J. Solid State Chem.* **34**, 65 (1980).
9. H. W. ZANDBERGEN, *J. Solid State Chem.* **35**, 367–375 (1981).
10. H. W. ZANDBERGEN, *J. Solid State Chem.* **37**, 308 (1981).
11. M. MEKATA AND K. ADACHI, *J. Phys. Soc. Japan* **44**, 806 (1978).

12. H. M. RIETVELD, *J. Appl. Crystallogr.* **2,** 65 (1969).
13. G. E. BACON, Compilation, Neutron Diffraction Newsletters, ed. W. B. Yelon, May 1977.
14. R. E. WATSON AND A. J. FREEMAN, *Acta Crystallogr.* **14,** 27 (1961).
15. H. T. WITTEVEEN, Thesis, Leiden (1973).
16. GUEN *et al., Rev. Chim. Miner.* **15,** 340 (1978).
17. S. J. SMART, "Effective Field Theories of Magnetism," Saunders, Philadelphia (1966).
18. D. W. WOOD AND N. W. DALTON, *J. Phys. C* **5,** 1675 (1972).
19. J. B. GOODENOUGH, "Magnetism and the Chemical Bond," Wiley–Interscience, New York (1963).
20. "International Tables for X-Ray Crystallography," Vol. II, p. 241, Kinoch Press, Birmingham.